Materials and Design 160 (2018) 455–467

Contents lists available at ScienceDirect

Materials and Design

journal homepage: www.elsevier.com/locate/matdes

Performance of multiphase scaffolds for bone repair based on two-photon polymerized poly(D,L-lactide-*co*-ε-caprolactone), recombinamers hydrogel and nano-HA

Reda M. Felfel [a,c,*], Dhanak Gupta [a,b], Adi Z. Zabidi [a], Amy Prosser [b], Colin A. Scotchford [a], Virginie Sottile [b], David M. Grant [a]

[a] Advanced Materials Research Group, Faculty of Engineering, University of Nottingham, UK
[b] Wolfson STEM Centre, School of Medicine, University of Nottingham, UK
[c] Physics Department, Faculty of Science, Mansoura University, Egypt

HIGHLIGHTS

- Fabrication of multiphase hybrids based on two-photon polymerised PLCL copolymer, Recombinamers Hydrogel and nano-HA.
- PLCL scaffolds exhibited instantaneous shape recovery after compression, a critical feature for arthroscopic delivery.
- PLCL scaffolds were shown to have accelerated degradation profiles in inflamed tissue mimic media (pH 4.5-6.5).
- The time-dependent degradation and compressive profiles of the hybrids suggested a surface erosion degradation mechanism.
- Cell viability assessment of hybrids with bone marrow derived human Mesenchymal Stem Cells showed no cytotoxic effects.

GRAPHICAL ABSTRACT

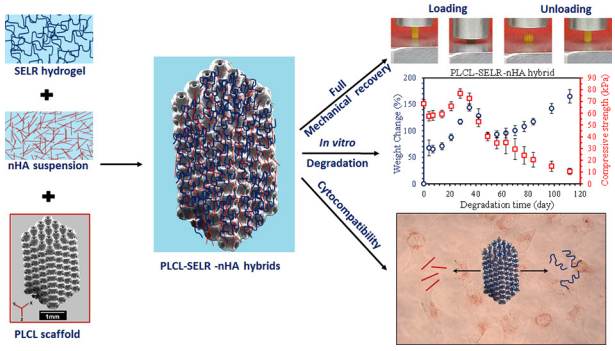

ARTICLE INFO

Article history:
Received 26 July 2018
Received in revised form 17 September 2018
Accepted 18 September 2018
Available online 19 September 2018

Keywords:
Poly(D,L-lactide-*co*-ε-caprolactone) copolymer
Multiphase hybrids
In vitro degradation
Mechanical recovery
human Mesenchymal Stem Cells

ABSTRACT

Multiphase hybrids were fabricated from poly(D,L-lactide-*co*-ε-caprolactone) (PLCL) copolymer scaffolds impregnated with silk-elastin-like recombinamers (SELRs) hydrogel containing 2 wt% hydroxyapatite nanoparticles (nHA). The PLCL scaffolds, triply-periodic minimal surface geometry, were manufactured using two-photon stereolithography. *In vitro* degradation studies were conducted on PLCL scaffolds in inflamed tissue mimic media (pH ~ 4.5–6.5) or phosphate buffered saline (PBS) at 37 °C. Compression test revealed instant shape recovery of PLCL scaffolds after compression to 70% strain, ideal for arthroscopic delivery. Degradation of these scaffolds was accelerated in acidic media, where mass loss and compressive properties at day 56 were about 2–6 times lower than the scaffolds degraded in PBS. No significant difference was seen in the compressive properties between PLCL scaffolds and the hybrids due to the order of magnitude difference between the hydrogels and the PLCL scaffolds. Moreover, degradation properties of the hybrids did not significantly change by inclusion of SELR+/−nHA nanocomposite hydrogels. The hybrids lost approximately 40% and 84% of their initial weight and mechanical properties, respectively after 112 days of degradation. Cytotoxicity assessment revealed no cytotoxic effects of PLCL or PLCL-SELR+/−2%nHA scaffolds on bone marrow-derived human Mesenchymal Stem Cells. These findings highlight the potential of these hybrid constructs for bone and cartilage repair.

* Corresponding author at: Advanced Materials Research Group, Faculty of Engineering, University of Nottingham, UK.
E-mail address: reda.felfel@nottingham.ac.uk (R.M. Felfel).

https://doi.org/10.1016/j.matdes.2018.09.035

1. Introduction

Natural polymers such as chitosan, collagen, gelatine and synthetic polymers, *e.g.* polylactic acid [1], polycaprolactone (PCL), polyglycolic acid (PGA), and their copolymers have been thoroughly investigated for a range of biomedical applications [2], from sutures and soft tissue grafting to load-bearing bone fixation devices [3]. Biocompatibility is a substantial characteristic for any implant material. However several other parameters such as degradation rate, swelling profile and mechanical performance in aqueous environments should also be carefully considered when selecting a biopolymer for an end application [4]. Natural and synthetic polymers have been fabricated into porous structures using a variety of methods such as porogen leaching, phase separation, freeze drying and electrospinning [2,3,5]. However, these techniques do not offer good control over geometry, porosity, pore size and strut thickness, which can significantly affect cell behaviour and fate [6,7]. Recently, 3D printing technologies have been introduced into the biomedical field to generate complex porous architectures with adjustable micro-features [8–10]. The 3D printing methods have typically used thermoplastics in the manufacture of synthetic polymer scaffolds due to their melt processing nature [9,10]. Alternatively, a thermoset or thermoplastic layer-by-layer approach (stereolithography) has also been applied using photo-polymerization of multifunctional monomers containing photoinitiators and acrylates reactive groups [9,11]. This method enables manufacturing of hierarchical polymer constructs with a well-defined geometry, porous structure and surface roughness of up to 5 μm resolution [10]. Further refinement using two-photon absorption (2PA) has been used in near-infrared (NIR) and visible light with femtosecond or picosecond pulsed laser to achieve higher writing resolutions of 100 nm [10,12]. More recently, scaffolds of PLA, PCL and polyethylene glycol (PEG) have been fabricated using 2PA stereolithography technology for biomedical purposes [10,12].

Copolymers of biodegradable polymers have been preferred over pure polymers as their degradation and mechanical profiles can be tuned *via* alteration of monomer ratios. Among all biodegradable copolymers, poly(D,L-lactide-*co*-ε-caprolactone) (PLCL) copolymer has potential. For example, PLCL copolymers have been utilized in development of elastic mechano-active scaffolds for tissue engineering such as cartilage repair [13,14]. In this work cell response was found to be enhanced within mechano-active scaffolds due to mechano-transduction [13]. Jeong et al. [15] investigated mechanical recovery of flexible scaffolds from PLCL copolymer. The scaffolds maintained nearly 96% mechanical recovery for two weeks in phosphate buffered saline solution (PBS) under cyclic tensile strain (ranged from 5 to 20%). PLCL scaffolds, having 300–500 μm pore size and 85% porosity, were also developed using a gel-pressing technique for cartilage regeneration in a rabbit model [16]. Deposition of chondral extracellular matrix was detected on the scaffolds, attributed to mechanical stimulation in the physiological environment of the rabbit. Therefore, the ideal scaffold should also maintain mechanical stability during the period of tissue healing while undergoing degradation and replacement by the remodelled tissue *in vivo* [15].

The manufacturing protocol, preliminary degradation and mechanical results of scaffolds fabricated with PLCL copolymer containing different ratios of lactide (LA) to ε-caprolactone (CL) (LC16:4, 18:2 and 9:1) through 2PA methods have been published [12]. Here, the degradation rates and compressive properties of the scaffolds were found to decrease as the CL content increased. This was ascribed to the slower degradation rate and low mechanical properties of PCL alone in comparison to poly(D,L-lactide) [12]. Such recoverable and degradable scaffolds may be an ideal platform for combination with injectable hydrogels such as elastin-like recombinamers (ELRs) to enhance cell response with scaffolds [17].

ELRs are synthetic polypeptides produced *via* genetic engineering technology to mimic natural elastin [18,19]. They are oligomeric macromolecules composed of a repeated amino acid sequence [19,20]. When Arg-Gly-Asp (RGD) and bone morphogenetic protein-2 (BMP-2) were incorporated into the ELR sequences, it boosted osteoinductivity and cell adhesion [21,22]. Semicrystalline blocks of silk can also be added to ELRs to produce silk-elastin-like recombinamers (SELRs) that combine the high strength of silk with the high elasticity of elastin, resulting in greater biological, degradation and mechanical properties [1,23,24]. *B. mori* silk is approved by the FDA as a biocompatible material and elastin is abundantly present in extracellular matrices of tissues. In addition, SELRs have proven to be biocompatible materials [1,23]. ELRs also have thermo-responsive properties; they convert from sol to gel *via* physical crosslinking at a transition temperature, which is usually lower than the body temperature (37 °C). Therefore, ELRs can be injected in the solution state and consequently gelled in the physiological environment [21]. The combined properties of biocompatibility, self-assembling conduct and mechanical strength make ELRs a good candidate for tissue engineering and drug delivery applications [18,20].

Hybrids of scaffolds impregnated with hydrogels have emerged to overcome the shortcomings of using scaffolds and hydrogels separately as an implant [25–27]. The hypothesis is that 3D porous scaffolds would provide mechanical integrity, support and geometry throughout the healing process of the tissue, while hydrogels would be a favourable environment for cell attachment, proliferation, differentiation, enabling easier exchange of nutrients and metabolic waste products with surrounding tissues [26–28]. The presence of hydrogel within the scaffold pores would also facilitate encapsulation of cells in cellularised implants [26]. However, only a few combinations of 3D printed polymer scaffolds and hydrogels have been studied such as, PCL-chitosan [26], PLA-gelatine [27], PCL/collagen -hyaluronic acid [29] and PCL-elastin [30]. Of these, a hybrid of 3D printed PCL scaffolds and chitosan hydrogel containing mesenchymal stem cells was prepared to explore their mechanical, degradation and osteogenic potential. The hybrid showed greater osteogenic differentiation and new bone-matrix formation after 2 weeks compared to PCL scaffold and chitosan hydrogel alone *in vitro* [26]. After 21 days in PBS, the degradation rate, percentage of wet weight change, of the hybrid was almost double the PCL scaffold and half the chitosan hydrogel. No significant change was seen in compressive properties of PCL scaffolds incorporated with hydrogel, which is to be expected due to significant mismatch between the mechanical properties of the PCL scaffold and chitosan hydrogel.

A further material can also be easily added into the hydrogel and subsequently in the hybrid structures. For example, nanoparticles have been encompassed into hydrogels to deliver supplementary functions to the multiphase hybrid constructs such as bioactivity [31], controlled-release [32] and drug delivery [33].

The research presented here combines these advantageous technologies to obtain a novel multiphase construct. Specifically, a well-defined 3D scaffold architecture was manufactured from PLCL copolymer using two photon polymerization (TPP) technology to the dimensions of $1.7 \times 1.7 \times 3.5$ mm^3. Cytotoxicity of the photoinitiators has been one of the complications associated with TPP [34]. A biocompatible photoinitiator (BA740) [35] was developed at University of Jena and used in the current study. The scaffolds were then impregnated with SELR hydrogel with or without 2 wt% of hydroxyapatite nanoparticles (nHA) [35]. The effect of SELR and SELR-nHA nanocomposite incorporation into PLCL unit cell scaffolds on the *in vitro* degradation, compressive and cytotoxic properties were investigated and presented here in a detailed study up to 112 days. The results showed that change in mechanical properties is strongly correlated with weight change profiles.

2. Materials and methods

2.1. Manufacture of PLCL unit cell scaffold

PLCL scaffolds were prepared by TETRA Society for Sensoric, Robotics and Automation GmbH and Institute for Bioprocessing and Analytical

Measurement Techniques (Germany), details of the scaffold fabrication methodology have been published earlier [12,35]. Briefly, ring opening polymerization process was used in synthesis of methacrylated lactic acid/ε-caprolactone (mLC) comonomer (LA:CL ratio of 16:4). The photoinitiator (BA740) was dissolved in acetone (0.2 mg μl^{-1}) and then added to the copolymer precursors to attain the concentration of 0.2%. The mixture was left continuously stirring overnight at 60 °C to remove the residual solvent and produce a uniform solution. M3DL TPP scanner setup (LZH Hannover, Germany) equipped with a source of femtosecond laser (140 fs, 80 MHz, 800 nm) was utilized for manufacturing PLCL scaffolds. The mLC and BA740 solution mixture was inserted between two glass coverslips separated by 2 mm using a spacer. The mLC solution was photo-polymerized using the laser beam that was adjusted in focus using a 63× objective lens with 0.75 optical aperture (LD-Plan-NEOFLUAR, Zeiss, Germany). A 3D nano-positioning stage controlled with computer model and supported by a galvanoscanner (Aerotech, USA) was used to control the track of the laser beam allowing for mLC materials to be polymerized in the 3D architecture. The laser intensity was adjusted at about 0.9 TW cm^{-2} and a writing velocity of 5 mm s^{-1} was used. Finally, the PLCL scaffolds were incubated for 24 h in acetone to eliminate the unpolymerised monomers. The Schwarz P unit cells of 520 μm size were printed and arranged in arrays to obtain scaffolds with the dimension of $1.7 \times 1.7 \times 3.5$ mm^3. The fabricated scaffolds (average molecular weight 1822 $g \cdot mol^{-1}$ [12]) were kept in double sterilization pouches and then gamma sterilized at the dose of 25 ± 2.5 kGy. The scaffolds remained in their pouches until testing.

2.2. Preparation of SELR-nHA nanocomposite hydrogel

Lyophilized SELR and suspension of nHA in PBS (2 wt%) were provided by The University of Valladolid and the Technical University of Catalonia, respectively (Spain). Details of preparation methodology and characterization of both SELR and nHA have been separately studied and published [1,23,24,36]. The nHA particles have a needle-like shape with approximately 100 nm in length [36]. SELR and nHA suspension were received sterilized and kept in −20 °C freezer prior to use. Their packages were opened and used inside a cell culture hood. SELR gel was reconstituted in PBS to a concentration of 100 mg ml^{-1}. The mixture was left continuously stirring for 6 h in an ice bath in order to maintain the temperature of the mixture to be below 4 °C, until the SELR was fully dissolved and a transparent uniform solution was obtained. The same method was followed to produce a SELR-nHA nanocomposite hydrogel with a nHA/PBS suspension. The solutions were cast into a plastic mould (see Supplementary information Fig. S1) and then left to allow physical crosslinking while kept in the mould at 37 °C for 4 days in 100% humid environment using a sealed plastic container containing PBS.

2.3. Preparation of PLCL-SELR-nHA multiphase hybrids

To impregnate the scaffolds with the hydrogel, SELR or SELR-nHA solutions were prepared as detailed above. The scaffold was initially inserted into a plastic micropipette tip and left to cool down to a temperature below 4 °C. Subsequently 70 μl of the hydrogel solution was injected onto the scaffold and the hydrogel was pushed forward and backward several times through the scaffolds using a 1 ml plastic syringe to ensure that the scaffold pores were fully occupied with the gel as graphically presented in Fig. 1. The tips contain PLCL-SELR or PLCL-SELR-2 wt% nHA were kept for 4 days at 37 °C and 100% humidity to allow the SELR hydrogel to physically crosslink. Finally, the hybrid samples were removed from the tip. Reconstitution and injection processes of the gel were performed in cell culture hood to maintain the sterilized state of the specimens and to allow for further tests.

2.4. Compression test of the multiphase hybrids

A Hounsfield testing machine with a 5 N load cell was used to measure the compressive properties of SELR and SELR-nHA nanocomposite hydrogels. A crosshead speed of 0.5 mm min^{-1} was applied on five replicates (n = 5) of the hydrogel specimens (4 mm diameter and 4 mm height) up to 20% compressive strain.

An Instron 5969 equipped with a 50 N load cell was used to evaluate compressive strength and modulus of the hybrids. Testing and calculations of compressive strength and modulus were performed in accordance to ASTM 1621-10: 2010. The hybrids were placed vertically between platens of the Instron and a crosshead speed of 0.5 mm min^{-1} was applied up to 20% strain. Measurements were conducted on five replicates (n = 5) of wet specimens. Before the start of degradation experiments, the initial compressive properties of the scaffolds were determined as wet after soaking in PBS for 60 min. Compressive strength was determined as the maximum compressive stress at 20% strain, while the modulus was calculated from the gradient of the initial part in the stress-strain curve.

To examine the mechanical recovery of the PLCL scaffolds, a loading-unloading hysteresis loop was measured for the dry samples up to 70% strain at the speed of 0.5 mm min^{-1} and a video was recorded for the whole test. Two successive cycles were applied on the same scaffolds with no time interval.

2.5. In vitro degradation studies

The standard, BS EN ISO 10993-13:2010 was followed to perform *in vitro* degradation experiments. An accelerated degradation experiment was conducted on PLCL scaffolds alone at 37 ± 1 °C using media at different pH values (7.4, 6.5, 5.5 and 4.5 ± 0.1). The pH of the degradation media was adjusted using diluted hydrochloride acid. Changes in weight, mass loss and pH of the degradation media were monitored against time for up to 56 days. In this experiment, the scaffolds (n = 5) were washed with distilled water and then blot dried with tissue paper before recording their wet weight. The dry weight of the scaffolds was obtained after drying at 50 °C for 120 min in a vacuum oven.

A further *in vitro* degradation experiment was conducted on PLCL scaffolds and PLCL-SELR+/−hybrids. Individual specimens were submerged in 30 ml of PBS (pH = 7.4 ± 0.1) using glass vials and kept in an oven at 37 ± 1 °C throughout the whole period of the study (112 days). At each degradation time points, the samples were removed from the degradation medium using a tweezer and shaken gently to remove surplus of PBS before determining the wet weight (m). Percentage changes in wet weight of the five replicates (n = 5) of each specimens were recorded against degradation time. Mass loss of the specimens was also determined as the percentage difference between the initial dry weight of the scaffolds and the dry weight of the samples after 112 days of degradation. Degradation media in both studies were replaced on a weekly basis.

2.6. Thermal analysis of SELR hydrogels

Differential thermal calorimetry (DSC, TA Q10) was used to determine the transition temperature (T_t) from solution into hydrogel. The test was conducted on fresh SELR (as prepared non-crosslinked) and crosslinked hydrogel (after maintaining at 37 °C and 100% humid environment for 4 days) over a temperature range of 5–50 °C with a heating and cooling rate of 5 °C min^{-1}.

2.7. Microscopic analysis

PLCL scaffolds and PLCL-SELR+/−nHA hybrids were sputter coated with platinum at 2.2 kV for 90 s using a Polaron SC7640 coater (Quorum Technologies, UK) and examined using JEOL 6400 scanning electron

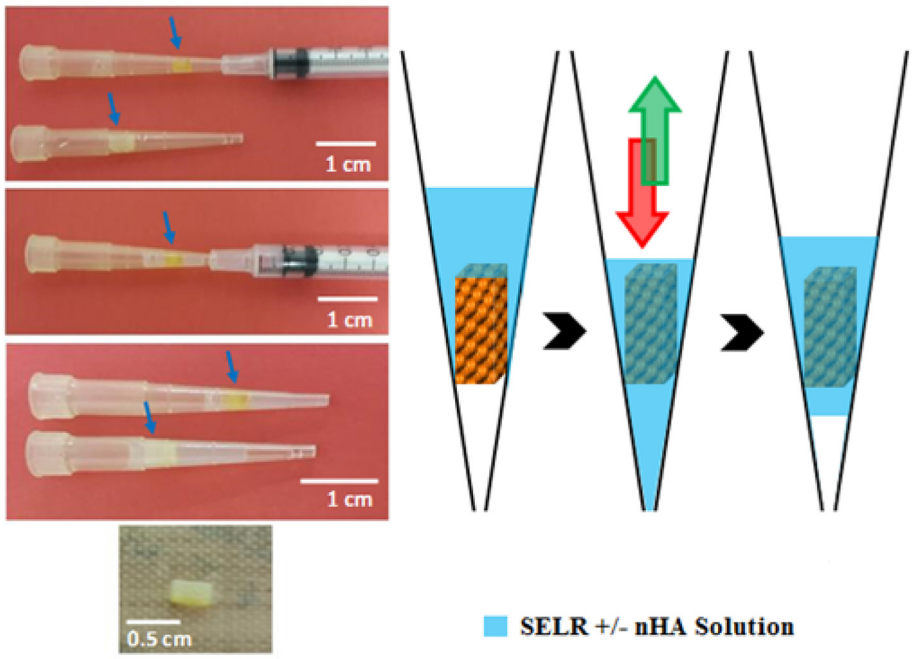

Fig. 1. Optical images and scheme for impregnation process of PLCL scaffold with SELR or SELR-2 wt% nHA nanocomposite hydrogels. Blue arrows point towards the scaffolds inside the micropipette tips. (For interpretation of the references to colour in this figure legend, the reader is referred to the web version of this article.)

microscopy (SEM) at 10 kV accelerating voltage and a working distance of 20 mm.

Optical images of PLCL scaffolds and PLCL-SELR+/−nHA hybrids were captured before and at the end of the degradation study (for wet and dry conditions) using a Nikon digital camera (Dxm1200F, Japan) attached to Nikon microscope (Japan). The images were processed using image analysis software (Nikon ACT-1 v. 2.62, LEAD Technologies, USA).

2.8. human Mesenchymal Stem Cell (hMSC) culturing

Reagents used were purchased from Thermo Fisher Scientific (UK) unless otherwise stated. Constitutively expressing Green Fluorescent Protein (GFP) adult human bone marrow-derived immortalized mesenchymal stem cells (hMSCs) were used in this study [37]. The cells were cultured in Dulbecco's Modified Eagle Medium (DMEM) supplemented with 10% (v/v) foetal calf serum (FCS), 1% (v/v) non-essential amino acids, 1 mM L-glutamine and 0.5% (v/v) Penicillin/Streptomycin, and maintained at 37 °C in a humidified atmosphere with 5% CO_2. At 70–90% confluency, the culture medium was removed; cells were then washed with phosphate saline buffer (PBS) and then harvested using 0.05% Trypsin-EDTA.

2.8.1. Cytocompatibility of SELR hydrogel

SELR was reconstituted to a concentration of 100 mg ml^{-1}, and allowed to set as a drop (100 μl volume) onto a culture coverslip for 40 min at 37 °C. A cell suspension of 4000 GFP-labelled hMSCs [37] was then added onto the coverslip and cell growth was monitored over 4 days by acquiring live cell imaging using JuLI™ FL (NanoEnTek, Korea).

2.8.2. Cytotoxicity evaluation of PLCL-SELR-nHA multiphase hybrids

By-products of the degradation of PLCL scaffolds and the hybrids were investigated according to ISO 10933-13. Individual specimens were fully immersed in 5 ml of DMEM inside a sterile 6-well plate and kept in an incubator (37 °C and 5% CO_2) for 28 days. DMEM without any specimens was used as control. After 7, 14 and 21 days of immersion, the DMEM conditioned with different scaffolds as well as the control (medium not exposed to scaffolds) was removed and replenished with fresh DMEM. The removed media was stored at −20 °C until testing.

The hMSCs were seeded at 2000 cells per well in a 96-well plate and after 24 h, culture medium was replaced with the control or conditioned DMEM from PLCL, PLCL-SELR and PLCL-SELR-2% nHA specimens after supplementation with 10% foetal calf serum and 1% of L-glutamine, non-essential amino acids and penicillin/streptomycin. Cells were incubated in conditioned medium for 24 h at 37 °C and 5% CO_2 in accordance with ISO 10993-5:2009 and then DNA content, cell metabolic activity and Neutral Red assays were performed as described below.

2.8.3. DNA content assay

The culture medium was removed and the cells were washed with PBS before adding 100 μl per well of sterile distilled water. Samples (n = 6) were lysed through three cycles of freeze thawing at −80 °C. DNA content was quantified using Quant-i™ PicoGreen® dsDNA Assay kit according to manufacturer's instruction. Briefly, each well was loaded with 100 μl of PicoGreen working solution (1 in 200 dilution of dye with 1× Tris-EDTA buffer). After a 5 min incubation period at room temperature, florescence intensity readings were taken on a Tecan Infinite M200 microplate reader (Tecan, UK) at 480 nm excitation and 520 nm emission. The DNA concentration was extrapolated using a standard curve prepared from standard DNA calf thymus provided with the assay kit. DNA content was expressed by normalizing against the control for each time point.

2.8.4. Cell metabolic activity assay

Metabolic activity of hMSCs was determined using PrestoBlue® assay. The culture medium was removed and cells were washed with PBS before adding 100 μl of PrestoBlue® working solution, which was prepared by mixing PrestoBlue® reagent with pre-warmed Hanks Balanced Salt Solution (HBSS) at a ratio of 1:9 (v/v). Six wells containing only PrestoBlue working solution with no cells were used as blanks. After 24 min the fluorescence intensity was measured at 530 nm excitation and 590 nm emission filters on a TECAN Infinite M200 micro-plate

reader. Cell metabolic activity was expressed after subtracting the reading for unreduced (blank) reagent and normalizing against the control at each time point.

2.8.5. Neutral Red uptake assay

For the stock solution, 0.2 g of Neutral Red (NR) (Sigma-Aldrich) was dissolved in 50 ml of sterile distilled water. NR solution was then diluted with DMEM at a ratio of 1 in 80 and syringe filtered using a 0.2 μm filter to remove insoluble dye crystals. For cell viability assessment, culture medium was removed and cells were washed with PBS before adding 100 μl of NR/DMEM solution to each well along with 6 blank wells. Samples were incubated for 3 h at 37 °C, 5% CO_2 before washing with PBS and subsequently blot drying the samples. At this stage images were taken using Nikon Eclipse TS100. To perform quantification, 100 μl per well of NR desorbing solution (1% glacial acetic acid, 49% ethanol and 50% water) was added to each well including the blank wells The well plates were gently shaken for 10 min and then NR absorption was measured at an optical density (OD) of 540 nm using a TECAN Infinite M200 micro-plate reader. Neutral Red uptake or cell viability was expressed after subtracting the reading for blank wells and normalizing against the control at each time point. Viability of <70% was considered to be cytotoxic as outlined by ISO 10993-5:2009.

2.9. Statistical analysis

At least five replicates ($n \geq 5$) of each specimen were used in all tests and the obtained results are represented as mean ± SEM (standard error), unless otherwise mentioned. GraphPad Prism software (version 6.0) or IBM SPSS Statistics 22 was used to perform statistical analysis. One-way ANOVA analysis with a *post hoc* Tukey comparison was applied for mechanical and degradation tests. For cytotoxicity, a two-way ANOVA was performed with the culture condition as a fixed factor and for post-hoc analysis, Least Significant Difference (LSD, equivalent to no adjustments) was carried out whereby P values <0.05 were considered significant.

3. Results and discussion

Hybrids consisting of hydrogels in polymer scaffolds have emerged as a natural development of implantable materials to exploit the combined characteristics of each individual constituent [3]. The 3D polymer scaffold would provide mechanical stability while hydrogels would offer hydrophilicity and good cell attachment [3,38]. Mechanical properties of polymer scaffolds can be adjusted through the alternation of porosity, polymer type and design of the construct [8]. Mechanical and biological properties of hydrogels could be also enhanced by incorporation of nanoparticles (*i.e.* nanocomposite hydrogel) such as hydroxyapatite [39,40]. In this study, a highly controllable 3D copolymer scaffold architecture was achieved using TPP, which were then infiltrated with SELR hydrogel with and without nHA particles. In order to investigate the mechanical performance of PLCL-SELR-nHA hybrids, compressive properties of PLCL scaffold, SELR and SELR-nHA were separately evaluated. The same composition and architecture of PLCL scaffolds alongside two other LA to CL ratios (18:2 and 9:1) were manufactured after which their degradation and mechanical properties were studied up to 90 days [12].

3.1. Mechanical recovery of the PLCL scaffolds

PLCL flexible scaffolds were tested up to 70% strain to examine their mechanical recovery, Fig. 2. Two identical narrow stress-strain hysteresis loops were obtained from two sequential loading-unloading cycles, indicating the lower energy dissipation during the loading-unloading cycles as a result of the high elasticity of the PLCL scaffolds [41]. The narrow hysteresis loops suggested also that the microstructural damage during the compression process of the PLCL scaffold was limited [41]. The high elasticity of the scaffolds was ascribed to the low glass transition temperature of PLCL copolymer (4.8 °C [12]). At room temperature (~20 °C), the PLCL copolymer is in its rubbery state. The stress-strain curve was linear up to 40% strain and the increase in the compressive stress afterwards (see Fig. 2) was attributed to the gradual compressing of the scaffold pores. Through a video recording (see Supplementary Movie S1) of the compression test (loading and unloading), it was found that the scaffold has fully recovered (100% of the original dimensions) within 5 min after 70% compressive strain. A second cycle of compression was then applied after it has fully recovered from the 1st cycle. It can be observed that the stress-strain loop between the 1st and 2nd cycle obtained was identical. This test evidenced the instantaneous shape recovery property of PLCL scaffolds and revealed their potential implementation in minimally invasive delivery (*i.e.* arthroscopic surgery) [42,43].

3.2. Accelerated in vitro degradation of PLCL scaffolds

Inflammatory responses normally initiated after occurrence of bone trauma are essential for bone healing [44]. Inflammation can last for a week after bone fracture and grafting [45,46]. Inflamed tissues are usually acidic with pH ranges from 6.0 to 7.0 or even lower than 6.0 [47]. The degradation rate of biodegradable polymers was found to be accelerated in acidic media [48]. In addition, photo-polymerization has been reported to change the degradation rate of polymers [49]. Therefore, it would be crucial to evaluate the stability of PLCL scaffolds in an acidic environment. Degradation and mechanical profiles of PLCL scaffolds were investigated in degradation media with different pH values (7.4, 6.5, 5.5 and 4.5 ± 0.1) at 37 °C, see Fig. 3. The weight change of scaffolds at lower pH (6.5, 5.5 and 4.5) initially increased up to 42% at day 3 and then decreased gradually to nearly −25% at day 56.Specimens with a pH of 7.4 showed a continuous increase over time, reaching up to 80% at day 42, followed by a gradual decrease to 50% at day 56, see Fig. 3a. The mass loss of scaffolds was determined after drying them in a vacuum oven for 120 min at 50 °C. The percentage of mass loss for all specimens (see Fig. 3b) increased gradually to 8% at day 28 with no significant difference being observed between scaffolds at different pH values. Afterwards, a significant difference was observed between scaffolds degraded in acidic media (pH from 4.5 to 6.5) and scaffolds in PBS (pH = 7.4). Initial increase in pH of the acidic degradation media to 7.4 at day 3 was followed by a steady decrease with increasing degradation time as shown in Fig. 3c. The initial increase in pH was suggested to be due to the leaching of chemical residuals as result of the scaffold fabrication process No significant difference was observed in terms of

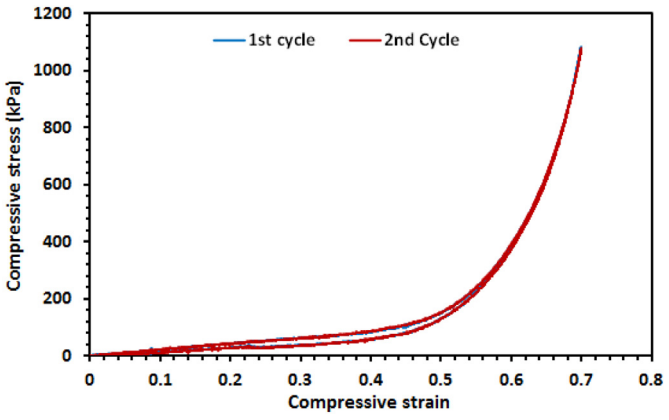

Fig. 2. Compressive loading-unloading hysteresis loop of the dry PLCL scaffolds, the compression test was applied on the scaffolds up to 70% strain at 0.5 mm min^{-1} speed and then unloaded to retrieve the original dimensions at the same speed. The scaffold exhibited an excellent recovery profile. Two successive cycles were applied on the same scaffolds and showed identical loops. (For interpretation of the references to colour in this figure legend, the reader is referred to the web version of this article.)

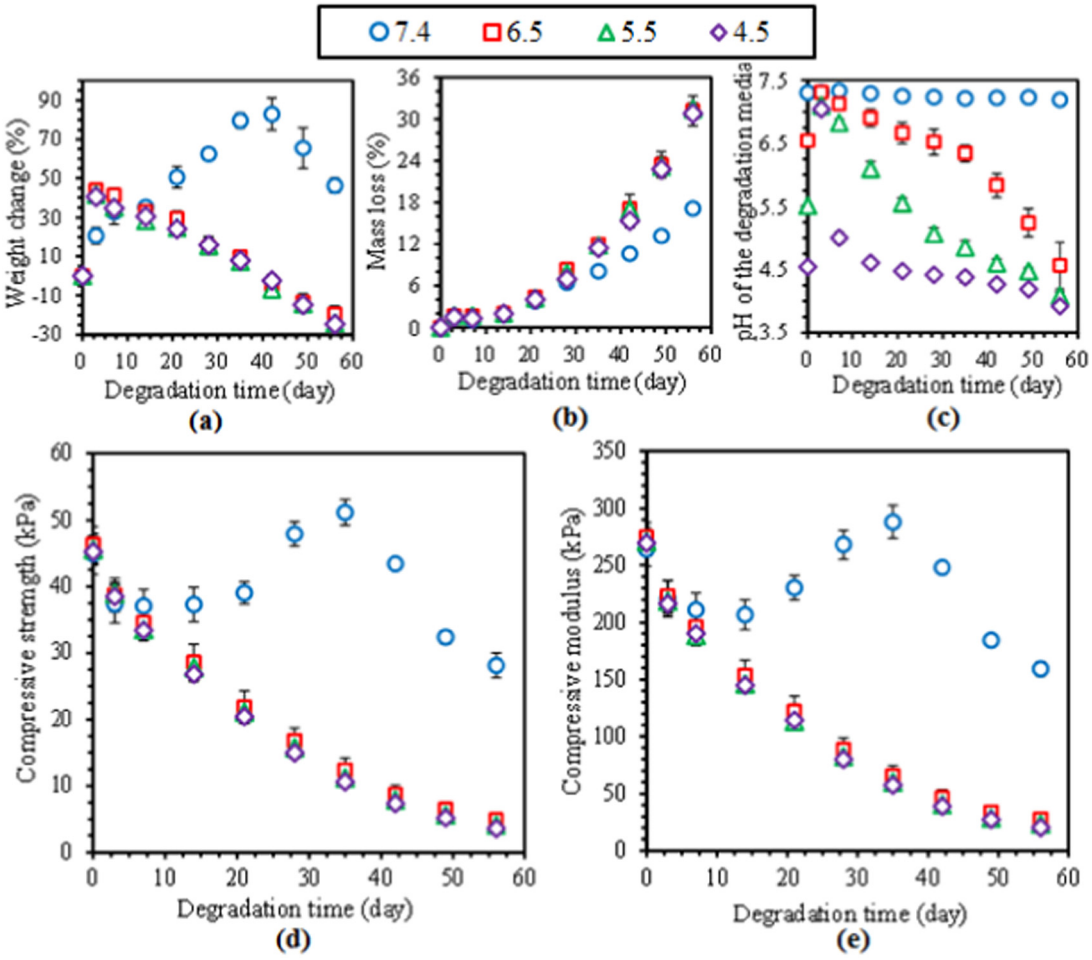

Fig. 3. Degradation and retention in compressive properties of PLCL scaffolds degraded in media of different pH values (7.4, 6.5, 5.5 and 4.5 ± 0.1); (a) percentage of weight change, (b) percentage of mass loss and (c) pH of degradation media changes against degradation time. Variation in compressive properties of PLCL scaffolds against time during degradation in media with different pH values (7.4, 6.5, 5.5 and 4.5) at 37 °C; (d) and (e) variation in compressive strength and compressive modulus of the degraded scaffold against degradation time. Five replicates (n = 5) were tested and error bars represent SEM. The degraded scaffolds in acidic media (pH of 6.5 and less) showed similar values and profiles (the differences in the properties are not significant, $P > 0.05$), which were different from scaffolds at pH of 7.4. (For interpretation of the references to colour in this figure legend, the reader is referred to the web version of this article.)

compressive properties between degraded scaffolds at different pH values up to day 7, followed by a significant decrease for scaffolds degraded at lower pH as shown in Fig. 3d and e. A late increase was seen in terms of compressive strength and modulus (50 kPa and 300 kPa, respectively) for specimens degraded at a pH of 7.4 after day 35. This may be due to the swelling of scaffolds as observed from Fig. 3a. Conversely, all the scaffolds with a pH value ranging between 6.5 and 4.5 revealed a continuous steady decrease in terms of their compressive properties, reaching up to a strength of 5 kPa and a modulus of 20 kPa at the end of the study (56 days) as result of progressive degradation of the scaffold materials, as shown in Fig. 3d and e. Alternatively, scaffolds degraded in PBS retained approximately 70% of their initial properties until day 56. This study could potentially explain the differences commonly observed between *in vitro* and *in vivo* degradation rates [50] since the presence of inflammation *i.e.* an acidic environment would accelerate the degradation of the implant and subsequently lead to an unpredictable degradation rate even if it was within a short period of time.

Changes in mass loss of scaffolds were similar up to 28 days, while differences in terms of their respective compressive properties when degraded in acidic media and PBS became significant on day 14. At day 28, the compressive strength and modulus for scaffolds degraded in PBS at a pH of 7.4 were three times greater than other groups. This was ascribed to the acceleration of degradation process of biodegradable polymers in acidic degradation media [51]. This outcome was also attributed to the nature of the degradation mechanism of bioresorbable polymers that initially involved reduction in molecular weight followed by a loss in terms of mechanical properties and weight loss [52]. The weight gain for the scaffolds degraded in PBS (pH 7.4) until 40 days was attributed to the swelling of the scaffolds and hence the increase in the amount of water uptake. The gradual (almost linear) change in mass loss and mechanical properties over time confirms that the scaffolds experienced a surface erosion mode of degradation [53]. Mondschein et al. [11] reported that the linear degradation profile of the scaffolds is indicative of surface erosion mechanism.

Changes in the degradation and mechanical properties of PLCL scaffolds in acidic media (pH of 4.5–6.5) *versus* time exhibited approximately the same values and trend ($P > 0.05$). Similar results for solid PLA specimens were reported by Lyu and Untereker [54]. The degradation rate of PLA did not change when the pH changed from 4 to 7 due to the low solubility of hydrogen (H^+) and hydroxide (OH^-) ions of the degradation media in the polymers [54].

3.3. Properties of SELR+/−nHA nanocomposite hydrogel

3.3.1. Thermal characterization of SELRs

As-prepared SELRs demonstrated reversible sol-gel phase change with transition temperatures (T_t) of 16 and 12 °C, endothermic and

exothermic peaks, from heating and cooling traces respectively, Fig. 4a and b. Differences between heating and cooling transition temperatures (thermal hysteresis of 4 °C) could be ascribed to the strong molecular interaction between SELR chains [55]. It is also highly dependent on heating/cooling rate, as the difference increases with increase in heating/cooling rate [56]. Below T_t, the SELR is in a solution state consisting of randomly disordered coils of ELR chains. As the temperature reaches T_t, the ELR chains self-assemble and fold resulting in its conversion into a gel state [57]. The exothermic peak during the cooling stage is attributed to the unfolding of the ELR chains [56]. Values of T_t depend on the molecular weight and presence of other molecules such *Bombyx mori* silk [1,57]. However, the reversible phase change and thermal transition characteristics of the hydrogel fully disappeared post thermal crosslinking. This was attributed to the self-assembling silk chains into thermally and chemically stable structure within the ELR hydrogels [1].

3.3.2. Mechanical influence of the nHA on SELR

The methodology for the synthesis and characterization of structural and biological properties of nHA have been previously published by Zhao et al. [36]. Fig. 4c and d show the compressive properties of SELR and SELR-2 wt% nHA nanocomposite hydrogels. Stress-strain curves for the SELR and SELR-nHA specimens (Fig. 4c) exhibited a nonlinear strain stiffening profile, where the stiffness of hydrogels increased as

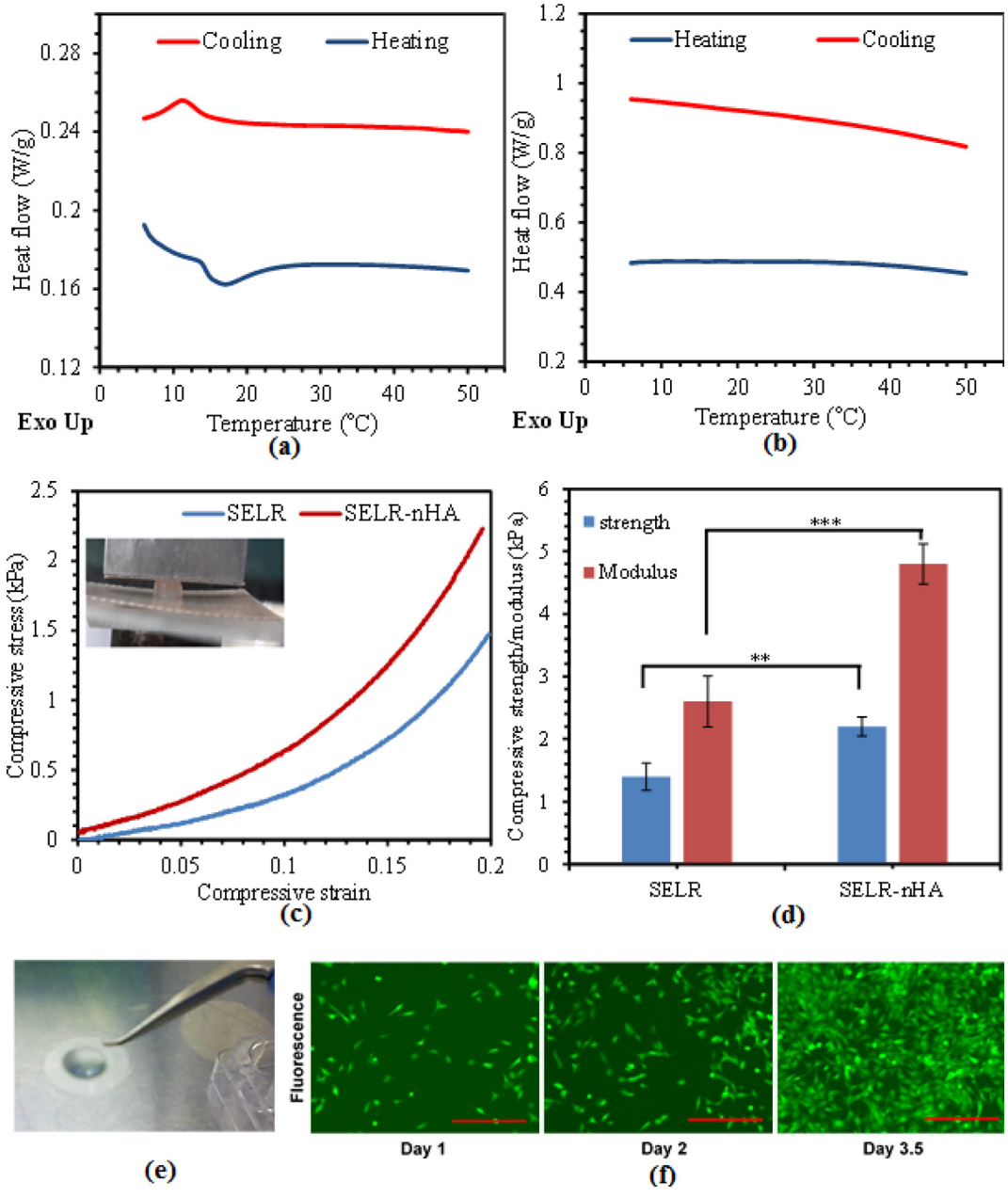

Fig. 4. Thermal, mechanical and cytocompatibility properties of SELR hydrogels; (a) and (b) represent heating-cooling DSC cycles for SELR hydrogels where (a) as-prepared hydrogel prior to crosslinking and (b) after thermally crosslinking y at 37 °C in 100% humid environment for 3 days. Compressive properties of SELR hydrogels before and after inclusion of 2 wt% nHA; (c) representative stress-stress curves and (d) compressive strength and modulus. At least five replicates (n = 5) of SELR+/−nHA hydrogels were tested and the mean values are presented (±SEM). GFP-labelled hMSCs were cultured with the SELR hydrogel; (e) preparation of the hydrogel for cell culture and (f) time-course of cells in culture after 1, 2 and 3.5 days in culture seen through FITC fluorescence channel (lower panel). Scale bar in Figure f equals 500 μm. ** and *** represent significant difference $P < 0.01$ and $P < 0.001$ respectively. (For interpretation of the references to colour in this figure legend, the reader is referred to the web version of this article.)

the applied compressive strain increased [58–60]. The strain stiffening property is common characteristic for natural hydrogels such as collagen, fibrin and actin [61]. This may be due to the anisotropic nature of the SELR hydrogel structure and the presence of silk fibroin [23,61]. Silk units are expected to provide mechanical stiffness to ELR hydrogels due to their high tensile strength [23,62]. Extracellular matrices of the tissue have been proven to follow a strain stiffness profile which was proposed to be essential to inhibit tearing of tissues under high stretching [63]. Incorporation of 2 wt% nHA led to a significant increase ($P < 0.01$) in the compressive strength and modulus of SELR hydrogels (*ca.* 60 and 85%, respectively) as shown in Fig. 4d. The agglomeration of nanoparticles was not anticipated since an aqueous suspension of as-prepared nHA was used in preparation of the nanocomposite hydrogels. Moreover, 1 wt% of tri-sodium citrate solution was added to the nHA suspension to aid optimum dispersion [36]. Note the organic component of the bone contains nearly 5.5 wt% of citrate [64].

3.3.3. Cytocompatibility of SELR hydrogel

GFP-labelled hMSCs seeded in the presence of SELR gels showed the ability to grow over time, displaying good adherence and interaction with the gels (see Fig. 4e and f). No significant cytotoxicity was observed, and cells reached confluence within a 3.5 day period. This finding supports previous studies [23,24] which concluded that SELRs support the proliferation of fibroblasts and mouse myoblast C2C12 cells while demonstrating cytocompatibility.

3.4. In vitro degradation of PLCL-SELR+/−nHA hybrids

Stress-strain curves for PLCL scaffolds and PCL-SELR+/−nHA hybrids approximately followed linear trends, see Supplementary information, Fig. S2a. As expected the PLCL scaffolds and PCL-SELR+/−nHA hybrids had similar mechanical properties as the order of magnitude larger properties of PLCL dominate, see Supplementary information Fig. S2b. A similar finding was reported for 3D printed PCL scaffolds and chitosan hydrogel hybrids containing MSCs [26].

PLCL scaffolds and PLCL-SELR+/−nHA hybrids exhibited consistent profiles in terms of changes in weight and pH of the degradation media (PBS) *versus* time throughout the whole duration of the study, see Fig. 5a and b. Furthermore, no significant differences ($P > 0.05$) in weight and pH changes were seen between PLCL scaffolds and the hybrid specimens. Similarities in weight change profiles was attributed to three reasons; all specimens were weighed in a wet state, the density

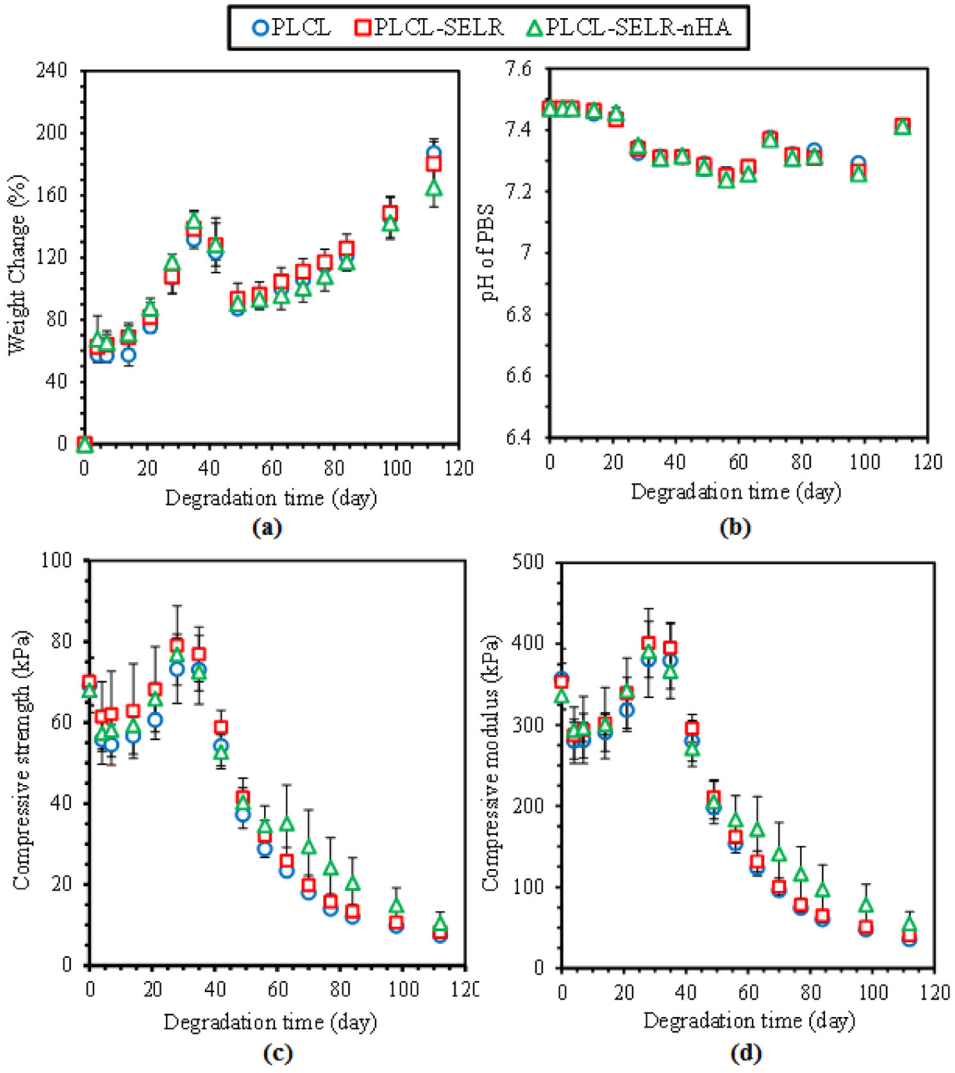

Fig. 5. In vitro degradation profiles of PLCL-SELR±2 wt% nHA hybrids in PBS at 37 °C; (a) variation in the weight against degradation time up to 112 days for the hybrids, (b) change in pH of the degradation medium against time and; (c) and (d) represent changes in compressive strength and modulus of PLCL-SELR+/−nHA hybrids against degradation time. Five replicates ($n = 5$) of each kind of specimen were tested and the mean was calculated (±SEM). The differences in weight, pH of degradation media, strength and modulus between PLCL, PLCL-SELR and PLCL-SELR-2 wt% nHA were not statistically significant ($P > 0.05$) throughout the whole degradation duration. (For interpretation of the references to colour in this figure legend, the reader is referred to the web version of this article.)

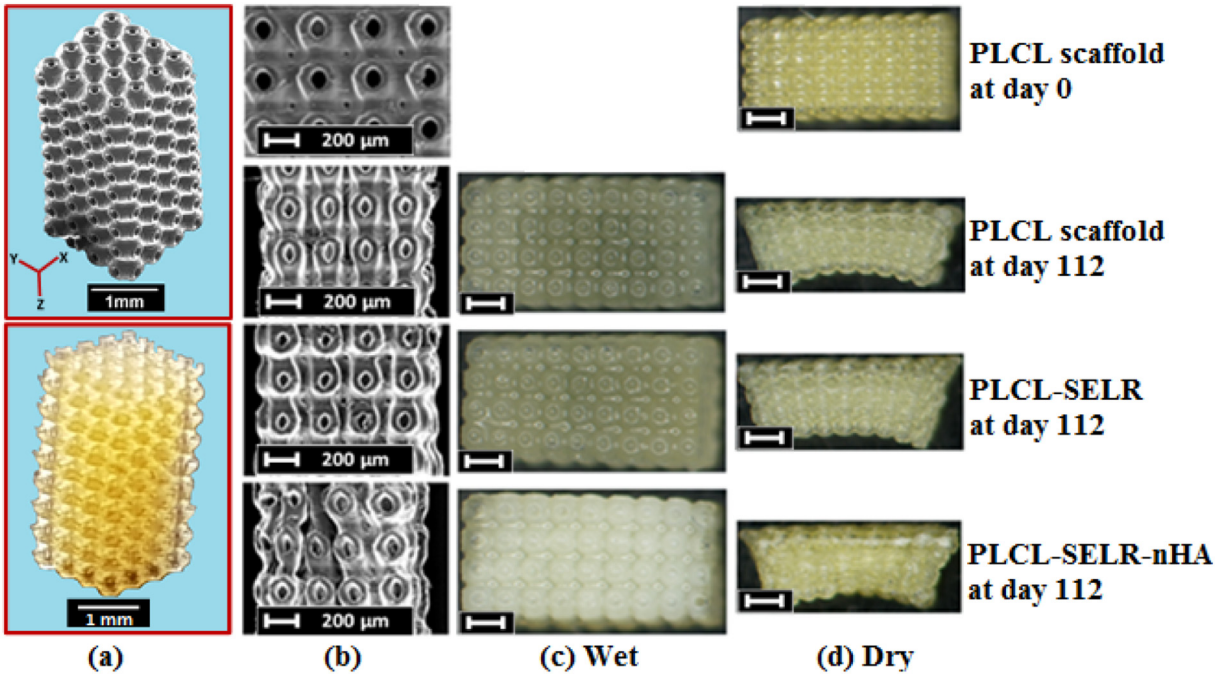

Fig. 6. Images for PLCL-SELR+/−nHA hybrids before (day 0) and after degradation in PBS at 37 °C for 112 days; (a) SEM and optical images of the 3D PLCL whole scaffolds (*ca.* 1.7 × 1.7 × 3.5 mm^3), (b) SEM micrographs for the dried specimens, (c) optical photographs for degraded hybrids (as wet) at day 112 and (d) optical micrographs for degraded hybrids after drying in a vacuum oven for 120 min at 50 °C. Scale bars in the optical images (c and d) equal 0.5 mm. (For interpretation of the references to colour in this figure legend, the reader is referred to the web version of this article.)

of hydrogels is very close to that of water [65] and the low degradation rate of SELR hydrogels [23]. Initial increase in the weight of all samples was due to water uptake reaching up to 140% at day 35. A significant decrease from 140% to 90% was observed between day 35 and day 49. This may be due to the leaching of unstable components from the scaffold material. A second swelling stage was then initiated and continued towards the end of degradation period at 112 days. PBS for all specimens remained neutral at 7.4 ± 0.2 throughout the duration of the experiment, see Fig. 5b. A previous study investigating similar scaffolds revealed that the pH of PBS remained neutral for up to 90 days even though the scaffolds lost approximately 40% of their initial weight [12]. In addition, the scaffolds degraded at 50 °C for 40 days lost >60% of their weight and no significant change was seen in the pH profile. This was ascribed to gradual degradation of scaffold materials, changing the degradation media on a weekly basis and the buffering capabilities of PBS [12]. The change in wet weight of the samples is a result of the opposing effects between two physical quantities *i.e.* the amount of water uptake and mass loss at each time point [66]. Therefore, increase weight change implies that the water uptake is dominant over mass and *vice versa*. At the beginning of degradation, water would diffuse into the scaffold material, resulting in a steep increase in the weight of the sample, until saturation is achieved. Afterwards, a balance between water uptake and mass is potentially achieved at some duration throughout the degradation study leading to an observable plateau in the plot for weight change against time [66].

Table 1
Final percentage changes in wet weight, swelling and mass loss of PLCL scaffold and PLCL-SELR+/−nHA hybrids at the end of the degradation experiment (112 day). The values presented in this table are mean of five replicates (±SEM).

Sample code	Weight change (%)	Swelling percentage (%)	Mass loss (%)
PLCL	187 ± 9	20 ± 2	41 ± 1
PLCL-SELR	180 ± 14	21 ± 3	38 ± 2
PLCL-SELR-nHA	165 ± 13	19 ± 3	43 ± 7

3.5. Mechanical retention of PLCL-SELR+/−nHA hybrids

Fig. 5c and d highlights changes in compressive strength and modulus for PLCL (as control), PLCL-SELR and the PLCL-SELR-nHA hybrids throughout the degradation period. No statistical significant differences ($P > 0.05$) in either strength or modulus were observed between different specimens at all time points. This was ascribed to the order of magnitude in the differences in mechanical properties between PLCL scaffolds and SELR+/−nHA hydrogels. The compressive strength and modulus of SELR+/−nHA hydrogels represent 3% or less of the scaffold. A similar finding was obtained for a hybrid of 3D printed PCL scaffolds and chitosan hydrogel [26]. However, the incorporation of the nanocomposite hydrogel into the scaffolds was intended to enhance their biological performance [40]. Compressive strength and modulus for all specimens initially decreased by about 20% at day 4, which was potentially due to plasticisation effects of PBS, followed by a gradual increase to 80 kPa and 400 kPa, respectively at day 28 due to scaffold swelling [12,67]. A gradual decrease was seen in both strength and modulus after 28 days reaching up to 10 MPa and 50 MPa, respectively, which was probably due to progressive degradation of the scaffold material. The gradual reduction in mechanical properties of the scaffolds confirms their degradation mechanism *via* surface erosion.

The 3D geometry of PLCL scaffolds can be observed from both SEM and optical images of the whole scaffold illustrated in Fig. 6a and b. SEM micrographs for PLCL, PLCL-SELR and PLCL-SELR-nHA hybrids before and after degradation are shown in Fig. 6b. Collapse and shrinkage of the scaffolds after degradation can also be observed. However, the scaffolds maintained the porous structure despite the pores being deformed. Swelling and enlarging of PLCL scaffolds throughout degradation experiments can also be seen from optical photographs of specimens before and after degradation as shown in Fig. 6c and d. Furthermore, the degraded scaffolds were clearly shrunk and deformed

after drying in a vacuum oven for 120 min at 50 °C, see Fig. 6d. The shrinkage of the scaffolds throughout the degradation process was reported to be an indication of surface erosion mechanism [11]. All the specimens had swelled by about 20% (their length increased from 3.5 mm to ~4.2 mm) after 112 days of immersion in PBS at 37 °C as tabulated in Table 1. The scaffolds and hybrid specimens lost approximately 40% of their initial weight after 112 days of degradation in PBS at 37 °C. This indicated that the samples followed a surface erosion degradation mechanism [53,68,69] which was attributed to the presence of a high fraction of interconnected pores and large surface area as well as minimal thicknesses of any sections of the TPP produced Schwarz unit cell. The high fraction of interconnected pores would facilitate the instantaneous release of degradation by-products. This has been confirmed from the pH profile which showed no sudden change in the pH of the degradation media towards the end of the study as shown in Fig. 5b. This can also due to the fact that PBS is capable to compensate the slight variations in the pH, buffering effect [12,67]. Late-inflammatory responses could occur due to change in local pH as a result of acidic degradation by-products [54]. This would be a preference in biomedical applications to obviate sudden failure of the implant and leaching of significant amounts of by-products as a result of acidic degradation [68] or excessive release of Ca^{2+} ions in the case of nHA incorporated hybrids, leading to cytotoxicity [70]. The white colour of the wet PLCL-SELR-nHA at the end of the degradation study verified the presence of the SELR hydrogel and nHA due to their slow biodegradability [23,71]. SELR is transparent, while the white colour is due to the presence of the hydroxyapatite nanoparticles.

3.6. Cytotoxicity assessment of PLCL and PLCL-SELR+/−nHA hybrids

To assess the cytotoxicity of PLCL, PLCL-SELR and PLCL-SELR-2 wt% nHA hybrids, proliferation, cell metabolic activity and Neutral Red uptake assays were performed using hMSCs cultured in medium conditioned with these scaffolds for 7, 14, 21 and 28 days.

The Neutral Red assay showed that cell viability is maintained in all conditions, indicating the lack of cytotoxicity as shown in Fig. 7a. There was no statistically significant difference between the different time-points analysed. In addition, metabolic activity of cells exposed to all conditioned media indicated maintained cell health, with no detectable loss upon exposure to material elutes (Fig. 7b). Cell numbers evaluated by DNA quantitation showed no apparent decrease upon exposure to conditioned medium (Fig. 7c). Overall, these results indicate that none of the test conditions were cytotoxic. This observation is in line with previous studies demonstrating non-toxic properties of PLCL, performed either *in vivo* or *in vitro* using different cells of mesenchymal origin. For example, 3D scaffolds made from PLCL/collagen (LA:CL = 50:50) allowed tendon-derived stem cells to grow and form extracellular matrices under mechanical stimulation *in vitro* or when implanted in nude mice or rabbit [72] Another study showed that adipose tissue derived stem cells (ADSCs) were found to adhere to 75:25 PLCL films alone without or with NaOH-HCl and fibronectin coating for end application in cell delivery for abdominal aortic aneurysms [73]; smooth muscle cells and endothelial cell were able to attach and grow on electrospun nanofibrous 75:25 PLCL scaffold for use as a blood vessel substitute [74]; rat bone marrow-derived MSCs were able to grow and express

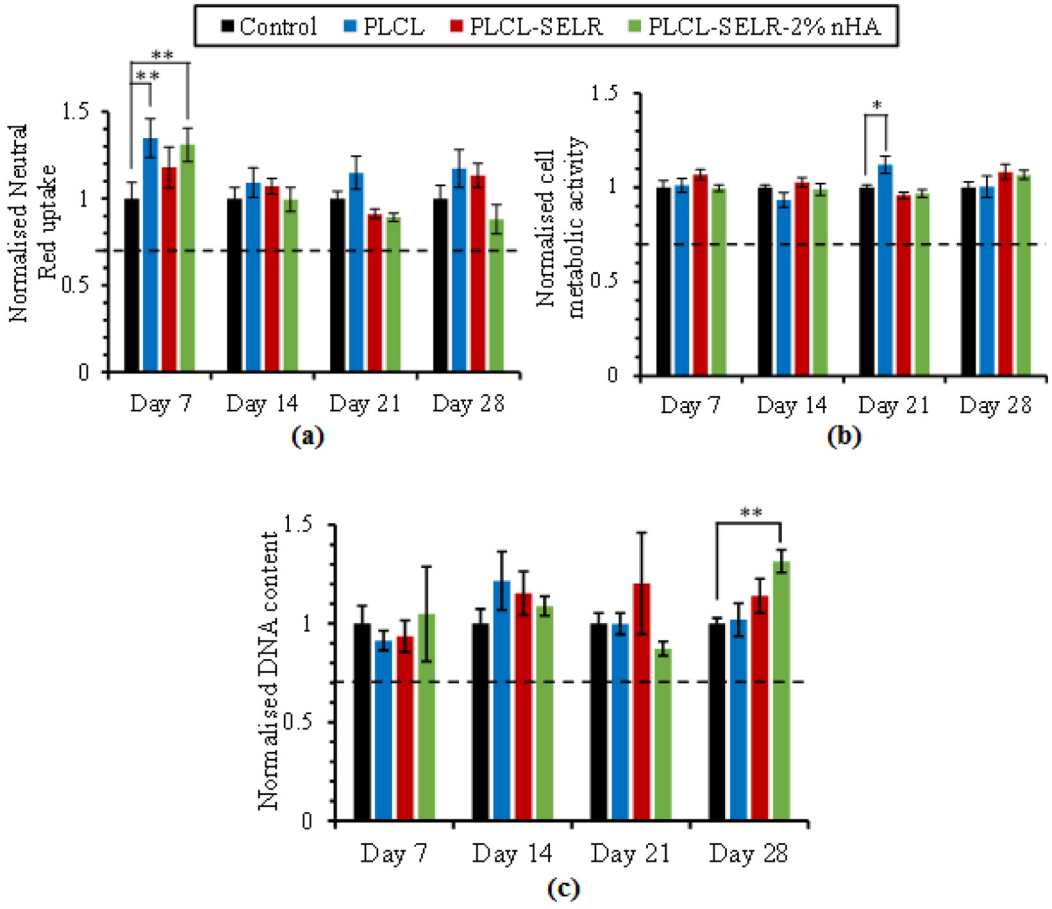

Fig. 7. Cytotoxicity assessment of PLCL, PLCL-SELR and PLCL-SELR –nHA hybrids using human mesenchymal stem cells. (a) Neutral red uptake, (b) metabolic activity and (c) DNA content measurements normalized to control (no scaffold control at each time point) after 24 h incubation in medium conditioned with different scaffolds for 7, 14,21 and 28 days. The dashed line indicates the 70% value compared to control. *P < 0.05 and **P < 0.01, n = 6, error bars represent standard error of mean (S.E.M.). (For interpretation of the references to colour in this figure legend, the reader is referred to the web version of this article.)

osteogenic markers significantly more on PLCL porous scaffolds compared to tissue culture polystyrene [75]; rat bone marrow-derived MSCs also showed no cytotoxic responses or alteration in mitochondrial when incubated with degradation products of PCL in PBS collected over 7, 14, 21 and 60 days [76]. Additionally, some previous studies have also reported the non-toxic nature of SELRs. Machado et al. [23] showed that when cell culture medium was supplemented with 2.5, 25 and 250 μg ml^{-1} of silk-elastin-like polymers, no cytotoxic effect on mouse myoblast cells (C2C12 cells) was observed after 5 days of culture. In another study, BJ-5ta (fibroblast) cells cultured for up to 3 days in medium conditioned with silk-elastin-like proteins electrospun with formic acid showed no cytotoxicity [23]. This suggests that copolymerization of lactic acid and caprolactone in PLCL scaffolds and subsequent impregnation with SELR+/−nHA did not promote release of acidic components such as lactic acid at toxic levels (>20 mmol l^{-1} in culture medium [77]), thereby maintaining physiological pH conditions (see Fig. 5b) allowing cell survival.

Although not detectable by the degradation study shown in Fig. 5a, there may be a very slow release of nHA from the PLCL-SELR+2 wt% nHA scaffolds during the 28 day incubation period in DMEM, as the size of the micro-sized pores within the hydrogel network are anticipated to be within a range of 4–200 μm [78], which is several magnitudes greater than the size of hydroxyapatite nanoparticles (100 nm in length with needle-like shape [36,33]). These particles may have either potentially been taken up by the cells *via* endocytosis and/or non-endocytic routes [33,79], subsequently degraded releasing Ca^{2+} in the cells; or these nanoparticles may have been degraded in the conditioned medium to release Ca^{2+} and then taken up by the cells [80], either way resulting in a positive effect on hMSC proliferation. Doses over 10 mM Ca^{2+} [81] in the culture medium are known to be cytotoxic, while lesser amounts have been shown to enhance MSC proliferation and osteogenic differentiation [80,81]. This could explain the significantly higher DNA content detected for PLCL-SELR-2 wt% nHA-conditioned medium compared to control medium ($P < 0.01$) on day 28 (Fig. 7c).

Interestingly, these results detected significantly higher cell viability at day 7 (Fig. 7a) for hMSCs cultured in medium conditioned with PLCL or PLCL hybrid scaffolds compared to control (with statistically significant differences in case of PLCL and PLCL-SELR-2% nHA, $P < 0.01$); and also significantly higher metabolic activity in case of hMSCs cultured in PLCL-conditioned medium compared to control ($P < 0.05$) at day 21. Previously, Serrano et al. [82] showed a slight increase in mitochondrial redox activity of L929 mouse fibroblasts cultured on PCL films. This however was not observable in the case of rat bone marrow-derived MSCs [76] when cultured in PCL extracts (in PBS) collected over 7, 14, 21 and 60 days of incubation. Alternately, the presence of lactic acid in conditioned medium may also have contributed to enhanced cell viability and mitochondrial activity. Lampe et al. [83] showed that lactic acid can scavenge harmful free radicals (generated as a result of photoinitiation) in culture medium in a dose dependent manner (0.1 to 5 mg ml^{-1}), and can improve the viability of neural precursor cells by 9–21%. The authors also showed that lactic acid can scavenge endogenous free radicals and reduce the intracellular redox state by increasing intracellular levels of pyruvate (involved in mitochondrial metabolism) and glutathione (part of cells natural antioxidant system).

In conclusion, the results indicated that the degradation products of PLCL and PLCL-SELRs+/−nHA scaffolds were not cytotoxic, suggesting that these scaffolds may be suitable for stem cell based therapeutic applications. In the future, direct contact cytocompatibility assessments of these scaffolds as well as osteogenesis and chondrogenesis assays will be performed to explore the benefits of these scaffolds for bone and cartilage repair.

4. Conclusions

Multiphase hybrid constructs were produced from a combination of well-defined 3D PLCL copolymer scaffolds, SELR hydrogels and hydroxyapatite nanoparticles. The PLCL flexible scaffolds exhibited total recovery after being fully compressed, which would enable future applications in minimally invasive delivery devices. The scaffolds also showed accelerated degradation in inflamed tissue mimic media through an acidic environment (pH 4.5–6.5). Mechanical and degradation properties of the hybrids did not significantly change through the inclusion of SELR or SELR-nHA nanocomposites, as a result of the substantial disparity between the mechanical properties of PLCL scaffolds and SELR hydrogels, as well as the slower biodegradability of the hydrogel. The gradual decrease in mechanical and mass loss over degradation time suggested scaffolds follow a surface erosion degradation mechanism attributed to the large surface area and minimal thickness of any section of the TPP produced Schwarz unit cell section. Surface erosion would be desirable for biomedical applications in order to eliminate the risks of sudden failure and late-inflammation due to burst of acidic degradation by-products. The PLCL scaffolds and the hybrids showed no evidence of cytotoxicity towards hMSCs. Consequently, these hybrid constructs represent potential new candidates for biomedical applications in regenerative medicine such as bone and cartilage repair.

Supplementary data to this article can be found online at https://doi.org/10.1016/j.matdes.2018.09.035.

Author contributions

R.M.F, D.G, A.Z.Z and A.P performed the measurements and data analysis; R.M.F and D.M.G designed the study; C.A.S, V.S and D.M.G planned and supervised the study; R.M.F and D.G drafted the manuscript and all authors discussed the results and commented on the manuscript.

Acknowledgements

The authors wish to thank our colleagues at the Institute for Bioprocessing and Analytical Measurement Techniques and TETRA Society for Sensoric, Robotics and Automation mbH (Germany) for providing the PLCL scaffolds and thank also Prof José Carlos Rodríguez-Cabello and Prof Maria-Pau Ginebra for providing SELR and nHA suspension as part of the EC FP7 InnovaBone project. This research project has received funding from the European Union's Seventh Framework Program (FP7/2007–2013) under grant agreement no. 263363. This work was supported by the Engineering and Physical Sciences Research Council [grant number EP/K029592/1]; and the EPSRC Centre for Innovative Manufacturing in Medical Devices (MeDe Innovation).

Data availability

The raw/processed data required to reproduce these findings cannot be shared at this time as the data also forms part of an ongoing study.

References

[1] W. Huang, A. Rollett, D.L. Kaplan, Silk-elastin-like protein biomaterials for the controlled delivery of therapeutics, Expert Opin. Drug Deliv. 12 (5) (2015) 779–791.
[2] A. Asti, L. Gioglio, Natural and synthetic biodegradable polymers: different scaffolds for cell expansion and tissue formation, Int. J. Artif. Organs 37 (3) (2016) 187–205.
[3] S. Stratton, N.B. Shelke, K. Hoshino, S. Rudraiah, S.G. Kumbar, Bioactive polymeric scaffolds for tissue engineering, Bioactive Mater. 1 (2) (2016) 93–108.
[4] A.J.T. Teo, A. Mishra, I. Park, Y.-J. Kim, W.-T. Park, Y.-J. Yoon, Polymeric biomaterials for medical implants and devices, ACS Biomater Sci. Eng. 2 (4) (2016) 454–472.
[5] T. Weigel, G. Schinkel, A. Lendlein, Design and preparation of polymeric scaffolds for tissue engineering, Expert Rev. Med. Devices 3 (6) (2006) 835–851.
[6] C.M. Bidan, K.P. Kommareddy, M. Rumpler, P. Kollmannsberger, P. Fratzl, J.W.C. Dunlop, Geometry as a factor for tissue growth: towards shape optimization of tissue engineering scaffolds, Adv. Healthc. Mater. 2 (1) (2013) 186–194.
[7] K. Worley, A. Certo, L. Wan, Geometry–Force Control of Stem Cell Fate, 2012.
[8] J. An, J.E.M. Teoh, R. Suntornnond, C.K. Chua, Design and 3D printing of scaffolds and tissues, Engineering 1 (2) (2015) 261–268.
[9] A.-V. Do, B. Khorsand, S.M. Geary, A.K. Salem, 3D printing of scaffolds for tissue regeneration applications, Adv. Healthc. Mater. 4 (12) (2015) 1742–1762.

[10] S.C. Ligon, R. Liska, J. Stampfl, M. Gurr, R. Mülhaupt, Polymers for 3D printing and customized additive manufacturing, Chem. Rev. 117 (15) (2017) 10212–10290.

[11] R.J. Mondschein, A. Kanitkar, C.B. Williams, S.S. Verbridge, T.E. Long, Polymer structure-property requirements for stereolithographic 3D printing of soft tissue engineering scaffolds, Biomaterials 140 (2017) 170–188.

[12] R.M. Felfel, P. Leander, G.-F. Miquel, M. Tobias, H. Gerhard, A. Ifty, S. Colin, S. Virginie, M.G. David, L. Klaus, In vitro degradation and mechanical properties of PLA-PCL copolymer unit cell scaffolds generated by two-photon polymerization, Biomed. Mater. 11 (1) (2016), 015011.

[13] Y. Yang, J.L. Magnay, L. Cooling, A.J. El Haj, Development of a 'mechano-active' scaffold for tissue engineering, Biomaterials 23 (10) (2002) 2119–2126.

[14] L. Chao, Z. Jingjing, L. Yijiang, M. Shamus, K. Gilson, G. Zigang, Poly (l-lactide-co-caprolactone) scaffolds enhanced with poly (β-hydroxybutyrate-co-β-hydroxyvalerate) microspheres for cartilage regeneration, Biomed. Mater. 8 (2) (2013), 025005.

[15] S.I. Jeong, B.-S. Kim, Y.M. Lee, K.J. Ihn, S.H. Kim, Y.H. Kim, Morphology of elastic poly (l-lactide-co-ε-caprolactone) copolymers and in vitro and in vivo degradation behavior of their scaffolds, Biomacromolecules 5 (4) (2004) 1303–1309.

[16] Y. Jung, M.S. Park, J.W. Lee, Y.H. Kim, S.-H. Kim, S.H. Kim, Cartilage regeneration with highly-elastic three-dimensional scaffolds prepared from biodegradable poly(l-lactide-co-ε-caprolactone), Biomaterials 29 (35) (2008) 4630–4636.

[17] D.L. Nettles, A. Chilkoti, L.A. Setton, Applications of elastin-like polypeptides in tissue engineering, Adv. Drug Deliv. Rev. 62 (15) (2010) 1479–1485.

[18] A. Girotti, A. Fernández-Colino, I.M. López, J.C. Rodríguez-Cabello, F.J. Arias, Elastin-like recombinamers: biosynthetic strategies and biotechnological applications, Biotechnol. J. 6 (10) (2011) 1174–1186.

[19] J.C. Rodríguez-Cabello, M.J. Piña, A. Ibáñez-Fonseca, A. Fernández-Colino, F.J. Arias, Nanotechnological approaches to therapeutic delivery using elastin-like recombinamers, Bioconjug. Chem. 26 (7) (2015) 1252–1265.

[20] J.C. Rodríguez-Cabello, L. Martín, A. Girotti, C. García-Arévalo, F.J. Arias, M. Alonso, Emerging applications of multifunctional elastin-like recombinamers, Nanomedicine 6 (1) (2011) 111–122.

[21] D.J. Coletta, A. Ibáñez-Fonseca, L.R. Missana, M.V. Jammal, E.J. Vitelli, M. Aimone, F. Zabalza, J.P.M. Issa, M. Alonso, J.C. Rodríguez-Cabello, S. Feldman, Bone regeneration mediated by a bioactive and biodegradable extracellular matrix-like hydrogel based on elastin-like recombinamers, Tissue Eng. A 23 (23–24) (2017) 1361–1371.

[22] M. Putzu, F. Causa, V. Nele, I.G.d. Torre, J.C. Rodriguez-Cabello, P.A. Netti, Elastin-like-recombinamers multilayered nanofibrous scaffolds for cardiovascular applications, Biofabrication 8 (4) (2016), 045009.

[23] M. Raul, C. André da, S. Vitor, G.-A. Carmen, M.C. Carlos, P. Jorge, G. Andreia, L.-M. Senentxu, R.-C. José Carlos, C. Margarida, Electrospun silk-elastin-like fibre mats for tissue engineering applications, Biomed. Mater. 8 (6) (2013), 065009.

[24] R. Machado, J. Azevedo-Silva, C. Correia, T. Collins, F.J. Arias, J.C. Rodríguez-Cabello, M. Casal, High level expression and facile purification of recombinant silk-elastin-like polymers in auto induction shake flask cultures, AMB Express 3 (1) (2013) 11.

[25] I. Hernandez, A. Kumar, B. Joddar, A bioactive hydrogel and 3D printed polycaprolactone system for bone tissue engineering, Gels 3 (3) (2017) 26.

[26] L. Dong, S.-J. Wang, X.-R. Zhao, Y.-F. Zhu, J.-K. Yu, 3D- printed poly(ε-caprolactone) scaffold integrated with cell-laden chitosan hydrogels for bone tissue engineering, Sci. Rep. 7 (1) (2017), 13412.

[27] M. Markovic, J. Van Hoorick, K. Hölzl, M. Tromayer, P. Gruber, S. Nürnberger, P. Dubruel, S. Van Vlierberghe, R. Liska, A. Ovsianikov, Hybrid tissue engineering scaffolds by combination of three-dimensional printing and cell photoencapsulation, J. Nanotechnol. Eng. Med. 6 (2) (2015) 0210011–0210017.

[28] I.M. El-Sherbiny, M.H. Yacoub, Hydrogel scaffolds for tissue engineering: progress and challenges, Glob. Cardiol. Sci. Pract. 2013 (3) (2013) 316–342.

[29] A.K. Ekaputra, G.D. Prestwich, S.M. Cool, D.W. Hutmacher, The three-dimensional vascularization of growth factor-releasing hybrid scaffold of poly (ε-caprolactone)/collagen fibers and hyaluronic acid hydrogel, Biomaterials 32 (32) (2011) 8108–8117.

[30] N. Annabi, A. Fathi, S.M. Mithieux, A.S. Weiss, F. Dehghani, Fabrication of porous PCL/elastin composite scaffolds for tissue engineering applications, J. Supercrit. Fluids 59 (2011) 157–167.

[31] J.R. Woodard, A.J. Hilldore, S.K. Lan, C.J. Park, A.W. Morgan, J.A.C. Eurell, S.G. Clark, M.B. Wheeler, R.D. Jamison, A.J. Wagoner Johnson, The mechanical properties and osteoconductivity of hydroxyapatite bone scaffolds with multi-scale porosity, Biomaterials 28 (1) (2007) 45–54.

[32] G.-H. Gwak, A.-J. Choi, Y.-S. Bae, H.-J. Choi, J.-M. Oh, Electrophoretically prepared hybrid materials for biopolymer hydrogel and layered ceramic nanoparticles, Biomater. Res. 20 (1) (2016) 1.

[33] S. Shah, P.K. Sasmal, K.-B. Lee, Photo-triggerable hydrogel-nanoparticle hybrid scaffolds for remotely controlled drug delivery, J. Mater. Chem. B 2 (44) (2014) 7685–7693.

[34] M. Tromayer, P. Gruber, M. Markovic, A. Rosspeintner, E. Vauthey, H. Redl, A. Ovsianikov, R. Liska, A biocompatible macromolecular two-photon initiator based on hyaluronan, †Electronic supplementary information (ESI) available. See DOI: 10.1039/c6py01787h Click here for additional data file Polym. Chem. 8 (2) (2017) 451–460.

[35] L. Poocza, M. Gottschaldt, E. Markweg, N. Hauptmann, G. Hildebrand, D. Pretzel, M. Hartlieb, C. Reichardt, J. Kübel, U.S. Schubert, O. Mollenhauer, B. Dietzek, K. Liefeith, Optimized photoinitiator for fast two-photon absorption polymerization of polyester-macromers for tissue engineering, Adv. Eng. Mater. 19 (3) (2017) (1600686-n/a).

[36] Z. Zhao, M. Espanol, J. Guillem-Marti, D. Kempf, A. Diez-Escudero, M.P. Ginebra, Ion-doping as a strategy to modulate hydroxyapatite nanoparticle internalization, Nanoscale 8 (3) (2016) 1595–1607.

[37] R. Harrison, H. Markides, R.H. Morris, P. Richards, A.J.E. Haj, V. Sottile, Autonomous magnetic labelling of functional mesenchymal stem cells for improved traceability and spatial control in cell therapy applications, J. Tissue Eng. Regen. Med. 11 (8) (2017) 2333–2348.

[38] G.D. Nicodemus, S.J. Bryant, Cell encapsulation in biodegradable hydrogels for tissue engineering applications, Tissue Eng. B Rev. 14 (2) (2008) 149–165.

[39] M. Biondi, A. Borzacchiello, L. Mayol, L. Ambrosio, Nanoparticle-integrated hydrogels as multifunctional composite materials for biomedical applications, Gels 1 (2) (2015) 162.

[40] S. Merino, C. Martín, K. Kostarelos, M. Prato, E. Vázquez, Nanocomposite hydrogels: 3D polymer–nanoparticle synergies for on-demand drug delivery, ACS Nano 9 (5) (2015) 4686–4697.

[41] H.-L. Gao, Y.-B. Zhu, L.-B. Mao, F.-C. Wang, X.-S. Luo, Y.-Y. Liu, Y. Lu, Z. Pan, J. Ge, W. Shen, Y.-R. Zheng, L. Xu, L.-J. Wang, W.-H. Xu, H.-A. Wu, S.-H. Yu, Super-elastic and fatigue resistant carbon material with lamellar multi-arch microstructure, Nat. Commun. 7 (2016), 12920.

[42] M. Montgomery, S. Ahadian, L. Davenport Huyer, M. Lo Rito, R.A. Civitarese, R.D. Vanderlaan, J. Wu, L.A. Reis, A. Momen, S. Akbari, A. Pahnke, R.-K. Li, C.A. Caldarone, M. Radisic, Flexible shape-memory scaffold for minimally invasive delivery of functional tissues, Nat. Mater. 16 (2017) 1038.

[43] S.A. Bencherif, R.W. Sands, D. Bhatta, P. Arany, C.S. Verbeke, D.A. Edwards, D.J. Mooney, Injectable preformed scaffolds with shape-memory properties, Proc. Natl. Acad. Sci. U. S. A. 109 (48) (2012) 19590–19595.

[44] M. Croes, M.C. Kruyt, L. Loozen, A.H. Kragten, H. Yuan, W.J. Dhert, F.C. Oner, J. Alblas, Local induction of inflammation affects bone formation, Eur. Cell. Mater. 33 (2017) 211–226.

[45] F. Loi, L.A. Córdova, J. Pajarinen, T.-h. Lin, Z. Yao, S.B. Goodman, Inflammation, fracture and bone repair, Bone 86 (2016) 119–130.

[46] P.M. Mountziaris, A.G. Mikos, Modulation of the inflammatory response for enhanced bone tissue regeneration, Tissue Eng. B Rev. 14 (2) (2008) 179–186.

[47] L. Dong, Z. Li, N.R. Leffler, A.S. Asch, J.-T. Chi, L.V. Yang, Acidosis activation of the proton-sensing GPR4 receptor stimulates vascular endothelial cell inflammatory responses revealed by transcriptome analysis, PLoS One 8 (4) (2013), e61991.

[48] H. Zhang, L. Zhou, W. Zhang, Control of scaffold degradation in tissue engineering: a review, Tissue Eng. B Rev. 20 (5) (2014) 492–502.

[49] J.D. Clapper, J.M. Skeie, R.F. Mullins, C.A. Guymon, Development and characterization of photopolymerizable biodegradable materials from PEG–PLA–PEG block macromonomers, Polymer 48 (22) (2007) 6554–6564.

[50] N. Bolgen, Y.Z. Menceloglu, K. Acatay, I. Vargel, E. Piskin, In vitro and in vivo degradation of non-woven materials made of poly(epsilon-caprolactone) nanofibers prepared by electrospinning under different conditions, J. Biomater. Sci. Polym. Ed. 16 (12) (2005) 1537–1555.

[51] F. Alexis, Factors affecting the degradation and drug-release mechanism of poly (lactic acid) and poly[(lactic acid)-co-(glycolic acid)], Polym. Int. 54 (1) (2005) 36–46.

[52] W.S. Pietrzak, D.R. Sarver, M.L. Verstynen, Bioabsorbable polymer science for the practicing surgeon, J. Craniofac. Surg. 8 (2) (1997) 87–91.

[53] R.P. Brannigan, A.P. Dove, Synthesis, properties and biomedical applications of hydrolytically degradable materials based on aliphatic polyesters and polycarbonates, Biomater. Sci. 5 (1) (2017) 9–21.

[54] S. Lyu, D. Untereker, Degradability of polymers for implantable biomedical devices, Int. J. Mol. Sci. 10 (9) (2009) 4033–4065.

[55] D. Kim, H. Kim, E. Lee, K.S. Jin, J. Yoon, Programmable volume phase transition of hydrogels achieved by large thermal hysteresis for static-motion bilayer actuators, Chem. Mater. 28 (23) (2016) 8807–8814.

[56] I. Galaev, B. Mattiasson, Smart Polymers: Applications in Biotechnology and Biomedicine, Second Edition CRC Press, 2007.

[57] J.C. Rodríguez-Cabello, L. Martín, M. Alonso, F.J. Arias, A.M. Testera, "Recombinamers" as advanced materials for the post-oil age, Polymer 50 (22) (2009) 5159–5169.

[58] M. Jaspers, M. Dennison, M.F.J. Mabesoone, F.C. MacKintosh, A.E. Rowan, P.H.J. Kouwer, Ultra-responsive soft matter from strain-stiffening hydrogels, Nat. Commun. 5 (2014) 5808.

[59] S. Skelton, M. Bostwick, K. O'Connor, S. Konst, S. Casey, B.P. Lee, Biomimetic adhesive containing nanocomposite hydrogel with enhanced materials properties, Soft Matter 9 (14) (2013) 3825–3833.

[60] Y. Pan, D. Xiong, Study on compressive mechanical properties of nanohydroxyapatite reinforced poly(vinyl alcohol) gel composites as biomaterial, J. Mater. Sci. Mater. Med. 20 (6) (2009) 1291–1297.

[61] C. Storm, J.J. Pastore, F.C. MacKintosh, T.C. Lubensky, P.A. Janmey, Nonlinear elasticity in biological gels, Nature 435 (2005) 191.

[62] R. Dandu, A.V. Cresce, R. Briber, P. Dowell, J. Cappello, H. Ghandehari, Silk–elastinlike protein polymer hydrogels: influence of monomer sequence on physicochemical properties, Polymer 50 (2) (2009) 366–374.

[63] J.P. Winer, S. Oake, P.A. Janmey, Non-linear elasticity of extracellular matrices enables contractile cells to communicate local position and orientation, PLoS One 4 (7) (2009), e6382.

[64] Y.-Y. Hu, A. Rawal, K. Schmidt-Rohr, Strongly bound citrate stabilizes the apatite nanocrystals in bone, Proc. Natl. Acad. Sci. 107 (52) (2010) 22425–22429.

[65] J.-M. Chern, W.-F. Lee, M.-Y. Hsieh, Preparation and swelling characterization of poly (n-isopropylacrylamide)-based porous hydrogels, J. Appl. Polym. Sci. 92 (6) (2004) 3651–3658.

[66] R.M. Felfel, K.M.Z. Hossain, A.J. Parsons, C.D. Rudd, I. Ahmed, Accelerated in vitro degradation properties of polylactic acid/phosphate glass fibre composites, J. Mater. Sci. 50 (11) (2015) 3942–3955.
[67] R.M. Felfel, I. Ahmed, A.J. Parsons, P. Haque, G.S. Walker, C.D. Rudd, Investigation of crystallinity, molecular weight change, and mechanical properties of PLA/PBG bioresorbable composites as bone fracture fixation plates, J. Biomater. Appl. 26 (7) (2012) 765–789.
[68] F.J. Buchanan, Degradation Rate of Bioresorbable Materials: Prediction and Evaluation, Woodhead Publishing, 2008.
[69] A. Göpferich, Mechanisms of polymer degradation and erosion, Biomaterials 17 (2) (1996) 103–114.
[70] G. Szabadkai, M.R. Duchen, Mitochondria: the hub of cellular Ca2+ signaling, Physiology 23 (2) (2008) 84–94.
[71] Y.X. Huang, J. Ren, C. Chen, T.B. Ren, X.Y. Zhou, Preparation and properties of poly (lactide-co-glycolide) (PLGA)/nano-hydroxyapatite (NHA) scaffolds by thermally induced phase separation and rabbit MSCs culture on scaffolds, J. Biomater. Appl. 22 (5) (2008) 409–432.
[72] Y. Xu, S. Dong, Q. Zhou, X. Mo, L. Song, T. Hou, J. Wu, S. Li, Y. Li, P. Li, Y. Gan, J. Xu, The effect of mechanical stimulation on the maturation of TDSCs-poly(L-lactide-co-e-caprolactone)/collagen scaffold constructs for tendon tissue engineering, Biomaterials 35 (9) (2014) 2760–2772.
[73] C.A. Burks, K. Bundy, P. Fotuhi, E. Alt, Characterization of 75:25 poly(l-lactide-co-epsilon-caprolactone) thin films for the endoluminal delivery of adipose-derived stem cells to abdominal aortic aneurysms, Tissue Eng. 12 (9) (2006) 2591–2600.
[74] C. Xu, R. Inai, M. Kotaki, S. Ramakrishna, Electrospun nanofiber fabrication as synthetic extracellular matrix and its potential for vascular tissue engineering, Tissue Eng. 10 (7–8) (2004) 1160–1168.
[75] S. Dånmark, A. Finne-Wistrand, M. Wendel, K. Arvidson, A.-C. Albertsson, K. Mustafa, Osteogenic differentiation by rat bone marrow stromal cells on customized biodegradable polymer scaffolds, J. Bioact. Compat. Polym. 25 (2) (2010) 207–223.
[76] V.S. S., P.V. M., Degradation of poly(ε-caprolactone) and bio-interactions with mouse bone marrow mesenchymal stem cells, Colloids Surf. B: Biointerfaces 163 (2018) 107–118.
[77] Y. He, W. Wang, J. Ding, Effects of L-lactic acid and D,L-lactic acid on viability and osteogenic differentiation of mesenchymal stem cells, Chin. Sci. Bull. 58 (20) (2013) 2404–2411.
[78] B. Kinikoglu, J.C. Rodríguez-Cabello, O. Damour, V. Hasirci, A smart bilayer scaffold of elastin-like recombinamer and collagen for soft tissue engineering, J. Mater. Sci. Mater. Med. 22 (6) (2011) 1541–1554.
[79] N.S. Remya, S. Syama, V. Gayathri, H.K. Varma, P.V. Mohanan, An in vitro study on the interaction of hydroxyapatite nanoparticles and bone marrow mesenchymal stem cells for assessing the toxicological behaviour, Colloids Surf. B: Biointerfaces 117 (2014) 389–397.
[80] G.-Y. Jung, Y.-J. Park, J.-S. Han, Effects of HA released calcium ion on osteoblast differentiation, J. Mater. Sci. Mater. Med. 21 (5) (2010) 1649–1654.
[81] S. Maeno, Y. Niki, H. Matsumoto, H. Morioka, T. Yatabe, A. Funayama, Y. Toyama, T. Taguchi, J. Tanaka, The effect of calcium ion concentration on osteoblast viability, proliferation and differentiation in monolayer and 3D culture, Biomaterials 26 (23) (2005) 4847–4855.
[82] M.C. Serrano, R. Pagani, M. Vallet-Regí, J. Peña, A. Rámila, I. Izquierdo, M.T. Portolés, In vitro biocompatibility assessment of poly(ε-caprolactone) films using L929 mouse fibroblasts, Biomaterials 25 (25) (2004) 5603–5611.
[83] K.J. Lampe, R.M. Namba, T.R. Silverman, K.B. Bjugstad, M.J. Mahoney, Impact of lactic acid on cell proliferation and free radical-induced cell death in monolayer cultures of neural precursor cells, Biotechnol. Bioeng. 103 (6) (2009) 1214–1223.